Available online at www.sciencedirect.com
ScienceDirect
Journal of Solid State Chemistry 180 (2007) 1894–1901
JOURNAL OF SOLID STATE CHEMISTRY
www.elsevier.com/locate/jssc

Order–disorder transition in the complex lithium spinel $Li_2CoTi_3O_8$

Nik Reeves*, Denis Pasero, Anthony R. West

Department of Engineering Materials, The University of Sheffield, Mappin Street, Sheffield, S1 3JD, UK

Received 21 March 2007; received in revised form 17 April 2007; accepted 26 April 2007
Available online 5 May 2007

Abstract

$Li_2CoTi_3O_8$ has an ordered $Li_2BB'_3O_8$ spinel structure, space group $P4_332$, at room temperature with 3:1 ordering of Ti and Li on the octahedral sites, and Li, Co disordered over the tetrahedral site. Rietveld refinement of variable temperature neutron powder diffraction data has shown an order–disorder phase transition in $Li_2CoTi_3O_8$ which commences at ~500 °C with Li and Co mixing on the tetrahedral and 4-fold octahedral sites and is complete at a first order structural discontinuity at ~915 °C. The fraction of Ti on the 12-fold octahedral site exhibits a small decrease with increasing temperature, which may suggest that the disordering involves all three cations. Above 930 °C, the structure, space group $Fd\bar{3}m$, has Li, Co and Ti sharing a single-octahedral site and Li, Co sharing a tetrahedral site, although Co still exhibits a preference for tetrahedral coordination. A labelling scheme for ordered and partially ordered 3:1 spinels is devised which focuses on the occupancy of the Li,*B* cations.

Keywords: Spinels; Ordered spinels; Cation ordering; Crystal structures; Neutron powder diffraction; Order–disorder; Phase transition

1. Introduction

Compounds with the spinel structure have been well studied [1–4]. The ideal spinel, Fig. 1, has a cubic close packed array of oxide anions, with an eighth of all tetrahedral interstices and half of all octahedral interstices filled by cations, space group $Fd\bar{3}m$. The arrangement of cations over these interstices can usually be explained using simple-crystal field theory or ionic radii arguments [2,4].

An extensive family of phases with an ordered spinel structure, space group $P4_332$, exists with 3:1 cation ordering on the octahedral sites [5–11]. This 3:1 ordering splits the 16*d* octahedral site into 4*b* and 12*d* sites and the 32*e* oxygen site into 24*e* and 8*c* sites (Fig. 2). These ordered 'ternary' phases have been less well studied, but their compositional versatility means that they are of interest as possible Li-ion battery electrode materials [8,10], solid electrolytes [7], and diluted magnets with possible spin glass states [12].

The ordered phases take the ideal formula $A_2BB'_3O_8$, where A = Li, B = Mg, Fe, Co, Ni, Cu or Zn, and B' = Ti, Ge or Mn. *A* and *B* are arranged over the 8-fold tetrahedral and 4-fold octahedral sites; B′ is isolated on the 12-fold octahedral site. The cation filling of the tetrahedral and 4-fold octahedral sites varies according to the metals used and can be rationalised using crystal field theory or cation size issues, as for AB_2O_4 spinels with $Fd\bar{3}m$ space group.

One ordered spinel phase that has received some attention is $Li_2CoTi_3O_8$. A complete range of spinel-like solid solution, $Li_{1.33x}Co_{2-2x}Ti_{1+0.67x}O_4$ ($0 \leqslant x \leqslant 1$) exists [12] and compositions $0.5 \leqslant x \leqslant 0.875$ exhibit 3:1 cation ordering with an ideal composition $x = 0.75$, i.e., $Li_2CoTi_3O_8$. Rietveld refinement [13] of room temperature X-ray powder diffraction data indicated that Co exhibited a strong preference for tetrahedral coordination [7,14,15]. Differential thermal analysis indicated a phase transition at ~909 °C, attributed to an order–disorder transition, as observed for analogous phases.

The aim of this work is to gain a better understanding of order–disorder phenomena in complex ternary spinels by analysing variable temperature neutron powder diffraction data. Here, we focus on $Li_2CoTi_3O_8$, and discuss changes

*Corresponding author. Fax: +44 114 222 5943.
E-mail address: n.reeves@sheffield.ac.uk (N. Reeves).

0022-4596/$ - see front matter © 2007 Elsevier Inc. All rights reserved.
doi:10.1016/j.jssc.2007.04.015

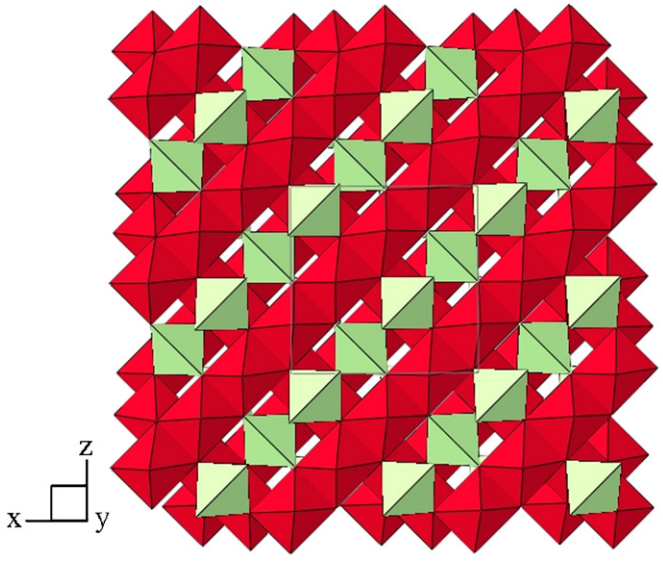

Fig. 1. Representation of the ideal spinel structure. AO_4 tetrahedra shown in light green, with BO_6 octahedra shown in red.

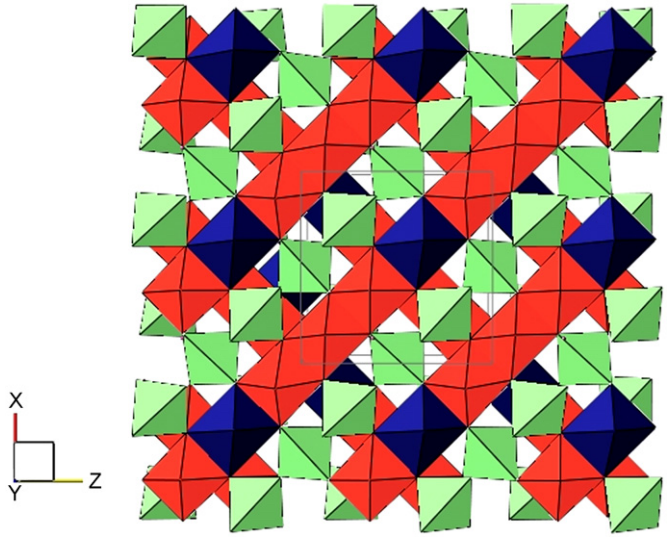

Fig. 2. Representation of the spinel structure with 3:1 cation ordering, space group $P4_332$. The tetrahedra around the 8*c* site are indicated in light green, the 4b octahedra in blue and the 12*d* TiO_6 octahedra in red.

in the cation distribution with temperature and the nature of the order–disorder phase transition.

2. Experimental

Reagents used were Li_2CO_3 (dried at 180 °C), TiO_2 (dried at 800 °C) and cobalt acetate ($Co(C_2H_3O_2)_2 \cdot 4H_2O$, assayed by TG to confirm water content). Stoichiometric amounts of the reagents were ground in an agate mortar and placed in Au 'boats' in a furnace at 120 °C. The temperature was increased slowly to 250 °C to allow decomposition of the acetate, to 650 °C for 3 h to decarbonate and to 850 °C for 45 h, with intermittent regrinding to complete reaction. The samples were then cooled slowly in the furnace to room temperature. Phase purity was checked using a STOE STADI P X-ray powder diffractometer in transmission mode with a position sensitive detector (PSD). A Ge(111) monochromator was used to give an intense monochromatic beam of Mo$K\alpha_1$ radiation ($\lambda = 0.70926$ Å).

Variable-temperature time-of-flight neutron powder diffraction, ND, data were collected on the POLARIS powder diffractometer at the ISIS Facility, Rutherford Appleton Laboratory, UK. For the data collected at 980 °C, the sample placed in a vanadium can was mounted within an evacuated high-temperature furnace; data collection times were ~2 h. At all other temperatures, the sample was placed in a glass capillary and measurements made in air; diffraction patterns were collected for 12 temperatures in total. Rietveld refinement used the EXPGUI [16] interface for GSAS [17] on data collected on the backscattering detector bank (d-range $0.2 \leqslant d/\text{Å} \leqslant 3.2$, resolution $\Delta d/d \sim 5 \times 10^{-3}$). The errors quoted for the refinement are as given by GSAS.

Thermogravimetry, TG, used a Perkin-Elmer Pyris 1 instrument in air, heating rate 10 °C/min. Differential scanning calorimetry (DSC) experiments used a Netzsch DSC404C in air, heating rate 3 °C/min and Pt crucibles.

3. Results and discussion

A phase-pure sample of green-coloured $Li_2CoTi_3O_8$ was obtained. The powder X-ray diffraction (XRD), pattern was fully indexed with $a = 8.37131(3)$ Å, space group $P4_332$. The ND patterns collected between 25 °C, Fig. 3, and 930 °C were also indexed on $P4_332$ since superstructure reflections, e.g. (411) and (322) at d-spacings of ~1.98 and 2.03 Å in Fig. 3 inset, were observed in addition to those expected for a spinel with space group $Fd\bar{3}m$. The intensity of these superstructure reflections remained approximately constant with temperature to 900 °C, but rapidly decreased thereafter and was essentially zero in the data collected at 980 °C, Fig. 4, which were indexed in the higher symmetry space group, $Fd\bar{3}m$.

The temperature dependence of the lattice parameters refined from ND and XRD (25 °C data point) data. Fig 5 shows a non-linear increase with temperature, with a gradual increase in da/dT.

4. Structural refinements

Rietveld refinements of $Li_2CoTi_3O_8$ were carried out using ND data collected at various temperatures. Two starting models were used, based on (i) a 3:1 cation 'ordered' model, $P4_332$ space group, with one tetrahedral site, 8*c*, two octahedral sites, 4*b* and 12*d*, and two oxygen sites, 8*c* and 24*e*; (ii) a cation disordered model, $Fd\bar{3}m$ space group, with cations filling the tetrahedral, 8*a*, and octahedral, 16*d*, sites, with a single oxygen site, 32*e*.

In model (i), the 8*c* site was half-filled by Li and half by Co, the 4*b* site was fully occupied by Li and the *12d* site

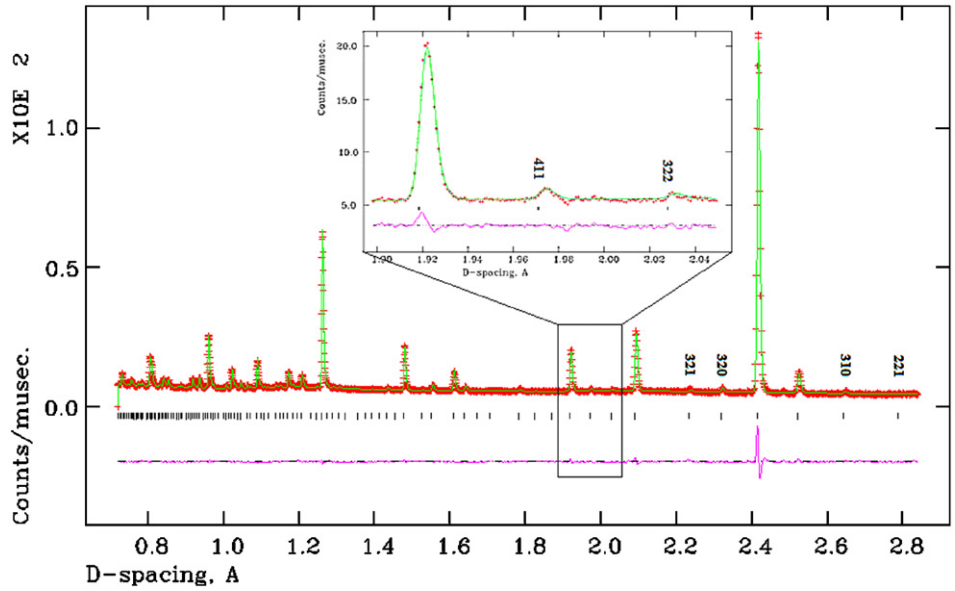

Fig. 3. Observed, calculated and difference fits from neutron powder diffraction data collected using the back scattered detector for $Li_2CoTi_3O_8$ at 25 °C. Indices are shown for superstructure peaks at high *d*-spacings.

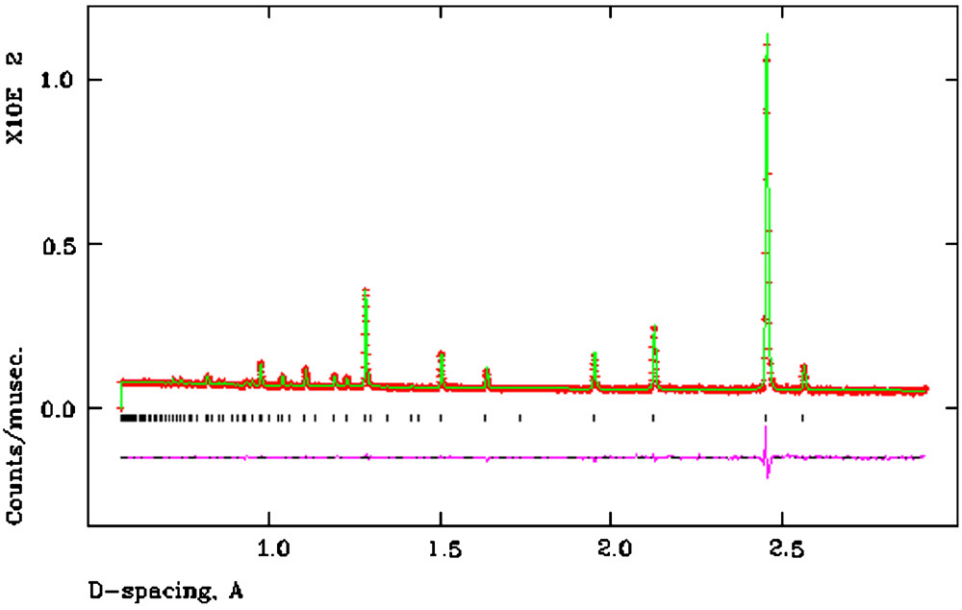

Fig. 4. Observed, calculated and difference fits from neutron powder diffraction data collected using the back scattered detector for $Li_2CoTi_3O_8$ at 980 °C.

fully occupied by Ti. Both 8*c* and 24*e* oxygen sites were fully occupied. In model (ii), Li and Co initially shared equally a fully occupied 8*a* site, with the 16*d* site filled by 0.25Li and 0.75Ti. The total occupancies for all sites were fixed to unity. Initial isotropic thermal parameters, U_{iso}s, were 0.025 $Å^2$ for all positions.

Several constraints were applied at the start of a refinement. The thermal parameters were constrained to be the same for all atoms sharing a particular site. The total occupancy of sites was set to unity. For the 16*d* site in model (ii), the sum of the fractional occupancies of Li and Co was fixed to 0.25, although initially no Co was placed on this site. The initial Ti fraction on this site was fixed at 0.75. No constraints were set between the occupancies of cations on different sites.

The background and scale factors were refined first, using a shifted Chebyschev function with 10 terms for the background, followed by the profile parameters. Atomic positions were refined in order of scattering length, regardless of sign, i.e., in the sequence O, Ti, and Co, Li together (as these always shared the same site). Finally, Li, Co and Ti site occupancies were refined, followed by thermal parameters. Where the refinement indicated that a site was shared by multiple cations, atomic coordinates,

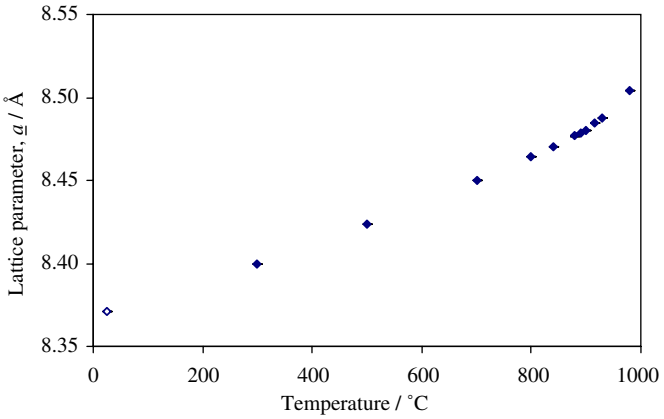

Fig. 5. Variation of lattice parameter, a, with temperature for $Li_2CoTi_3O_8$. Estimated standard deviations are smaller than the data points. Lattice parameters are calculated from X-ray (◇) and neutron (◆) powder diffraction data.

thermal parameters or fractions were refined simultaneously as appropriate. The whole process was repeated to convergence with negligible shifts in atomic variables. The statistics observed for all refinements were relatively good, with $\chi^2 \leqslant \sim 3$ in all cases and discrepancy, or R, values always less than 6%. The visual fit of the data was good in all cases. The final parameters and bond lengths at 25, 700 and 980 °C are given as examples in Table 1; example final profile fits are given in Figs. 3 and 4. A summary of the refinement results is given in Table 2.

On refining the Li and Co fractions on the 8*c* and 4*b* sites at 25 °C, the change away from the fully ordered arrangement was significantly less than 1 esd, and so the fractions were fixed according to the fully ordered cation arrangement with only Li on the 4*b* site, and 0.5 Li/0.5 Co on the 8*c* site. For several refinements of data collected below 980 °C, it was possible to refine stable atomic coordinates for the 8*c* site, which did not change significantly with temperature, and occupancies and thermal parameters for both 8*c* and 4*b* sites.

The fraction of Li and Co on the tetrahedral site altered significantly with temperature (Fig. 6). With the overall site occupancy constrained to unity, the Li fraction on this site increased progressively rapidly with temperature and was matched by a decrease in Li occupancy of the 8*c* site, (Fig. 7). Note that at 980 °C, the 16*d* site is occupied by 0.75 Ti and 0.25 (Li + Co); to allow comparison with lower temperature data, the Li occupancy at 980 °C was normalised (by quadrupling).

The 12*d* site has so far been considered occupied solely by Ti, but it is plausible that Ti may have a role in the disordering process. However, the refinement of three cation occupancies on one crystallographic site is not trivial in GSAS, and it is hard to constrain atoms in any meaningful way. Therefore, refinement of only the Ti occupancy on the 12*d* site was attempted; results for a number of temperatures. Fig 8 shows a slight decrease in Ti occupancy with temperature. Including very small fixed amounts (<1%) of Ti on the other crystallographic sites did not yield any improvement in statistics or stability of the refinements. For 980 °C data, refinements were also attempted with only Ti on the 16*d* site, with starting occupancy of 0.75 and U_{iso} set to a reasonable value of 0.025 Å^2; when refined, the occupancy increased slightly, to 0.784(5), indicating that this site wanted an increased amount of scattering, which is in good agreement with what would be expected from having an approximately 4:1 mix of Li and Co filling the remainder of the site, as in the final refinement (Table 1).

The thermal parameters for the 8*c* site became slightly negative in refinements of data collected at 840 °C (−0.003(7)) and 880 °C (−0.009(18)) but within one esd were statistically indistinguishable from positive values. In data sets collected at 900, 915 and 930 °C, a complete structural refinement could not be made: it was not possible to refine fractional coordinates, occupancies and thermal parameters for the tetrahedral site as the model would not converge.

For the data sets collected at temperatures where satisfactory full refinements were made, stoichiometries based on the refined cation arrangements were calculated (Table 1). Within 1–2 esds, there is no change in refined stoichiometry with temperature.

5. Thermal analysis

TG experiments (not shown) showed no weight loss for $Li_2CoTi_3O_8$ on heating to 1000 °C in air, in agreement with previous reports [7]. DSC carried out on $Li_2CoTi_3O_8$ showed, Fig. 9, a sharp endotherm at ~915 °C on heating; this was reversible on cooling with a small hysteresis, at 890 °C. The sharp nature of the peaks suggests that this may be a first-order transition.

6. Discussion

Rietveld refinement of neutron PD data shows that at 25 °C, $Li_2CoTi_3O_8$ exhibits 3:1 ordering on the octahedral sites. The data collected at temperatures up to 930 °C fit the $P4_332$ space group, though the intensity of the superstructure reflections diminishes with increasing temperature above 900 °C. Calculated bond lengths, Table 1 shows a small distortion in both the 8*c* tetrahedra and 12*d* octahedra; the 4*b* octahedra are undistorted. The bond lengths are in reasonable agreement with expected values [18], and appropriate for spinel oxides. In general, the bond lengths increase with temperature (Fig. 10). The exception to this is the 8*c*–O(1) bond, which decreases significantly, reaching 1.792(1) Å at 880 °C. Typical Li–O bond lengths can vary greatly for a tetrahedral arrangement, e.g., in lithium orthosilicate, Li_4SiO_4, Li–O bond lengths vary over the range ~1.9–2.2 Å [19]. However, in the present study it is noted that the esds on the refined 8*c* site position increase with temperature and are significantly larger than for the other sites; in addition, the refined U_{iso}'s for the *8c* site

Table 1
Structure refinement parameters, refined stoichiometries and bond lengths for $Li_2CoTi_3O_8$ at 25, 700 and 980 °C

	Temperature/°C		
	25	700	980
Space group	$P4_332$	$Fd\bar{3}m$	$Fd\bar{3}m$
a, Å	8.37131 (3)	8.45024 (4)	8.50402 (4)
V, Å^3	586.652 (6)	603.403 (8)	614.997 (9)
χ^2	2.90	2.01	1.57
wRp (%)	2.71	3.32	4.02
Rp (%)	4.61	4.65	5.32
Refined stoichiometry	$Li_2CoTi_3O_8$	$Li_{1.97(3)}Co_{1.03(3)}Ti_3O_8$	$Li_{1.95(4)}Co_{1.05(4)}Ti_3O_8$
Tetrahedral Site	8*c*	8*c*	8*a*
Site occupancy	0.5 Li/0.5 Co	0.520 (6) Li/0.480 (6) Co	0.588 (7) Li/0.412 (7) Co
x ($= y = z$)	0.9980 (27)	0.9889 (4)	0.125
U_{iso}, Å^2	0.0103 (32)	0.0088 (83)	0.025
Octahedral site 1	4*b*	4*b*	
Site occupancy	1.0 Li/0.0 Co	0.933 (14) Li/0.067 (14) Co	
x ($= y = z$)	0.625	0.625	
U_{iso}, Å^2	0.0333 (30)	0.0334 (22)	
Octahedral site 2	12*d*	12*d*	16*d*
Site occupancy	1.000 (4) Ti	0.988 (6) Ti	0.193 (6) Li/0.057 (6) Co/0.750 Ti
x	0.125	0.125	0.5
y	0.3679 (2)	0.3688 (3)	0.5
z	0.8821 (2)	0.8811 (3)	0.5
U_{iso}, Å^2	0.0109 (4)	0.0229 (3)	0.0282 (6)
O(1)	8*c*	8*c*	32*e*
Site occupancy	1.0 O	1.0 O	1.0 O
x ($= y = z$)	0.3895 (1)	0.3896 (2)	0.26299 (4)
U_{iso}, Å^2	0.0131 (3)	0.0178 (4)	0.0272 (2)
O(2)	24*e*	24*e*	
Site occupancy	1.0 O	1.0 O	
x	0.1059 (1)	0.1034 (2)	
y	0.1272 (1)	0.1284 (1)	
z	0.3905 (1)	0.3919 (1)	
U_{iso}, Å^2	0.0113 (2)	0.0210 (3)	
Bond lengths			
Tet.—O(1)	1.995 (1) (× 1)	1.880 (1) (× 1)	2.033 (1) (× 4)
	1.982 (1) (× 3)	2.060 (1) (× 3)	
Oct. 1—O(2)	2.121 (1) (× 6)	2.153 (1) (× 6)	
Oct. 2—O(1)	2.035 (1) (× 2)	2.046 (1) (× 2)	2.022 (1) (× 6)
Oct. 2—O(2)	1.977 (1) (× 2)	1.985 (1) (× 2)	
	1.883 (1) (× 2)	1.893 (1) (× 2)	

decrease with increasing temperature, and are negative in refined data from 840 and 880 °C. It may be that the Li and Co are for some reason uncomfortable sharing the same site, and are diverging onto two discrete but closely separated crystallographic sites; the results here may be an averaging of two such sites.

The cation ordering is absent from data collected at 980 °C, where the data can be fitted with the $Fd\bar{3}m$ space group. This correlates with the phase transition observed by DSC, where a sharp endotherm suggests a first-order phase transition at ~915 °C. Such order–disorder transitions have been reported previously for analogous complex lithium spinels [7,20].

The Rietveld refinements show significant mixing of Li and Co on the 8*c* (tetrahedral), Figs. 6 and 4b (octahedral), Fig. 7, sites at temperatures above 500 °C. The degree of mixing increases with temperature. Although the sum of the fractions of Li and Co on each crystallographic site was constrained to unity, there was no constraint between different crystallographic sites in terms of overall Li content, Co content, or Li/Co content. The refined stoichiometries, Table 1, are relatively unchanged, despite the large shifts in Li and Co contents between sites. The deviation from linearity in the temperature dependence of lattice parameters is probably related to this cation mixing. The refined composition at 980 °C is still that of the stoichiometric phase within errors; any change in stoichiometry due to possible loss of volatile species (Li, Co and/or O) induced by the extreme conditions is limited.

Table 2
Summary table showing key changes in refinement results with increasing temperature

Temperature	Space group	Tetrahedral sites	Octahedral sites		Oxygen sites	
Ambient	$P4_332$	8*c*	4*b*	12*d*	8*c*	24*e*
		(0.5Li / 0.5Co)	(1.0Li)	(1.0Ti)		
Effect of increasing temperature		Li/Co ratio increases. Tetrahedral distortion increases. Uisos become negative, higher esds.	Co/Li ratio increases.	Small decrease in Ti occupancy		
980 °C	$Fd\bar{3}m$	8*a*	16*d*		32*e*	
		(0.588Li / 0.412Co)	(0.19Li / 0.06Co / 0.75 Ti)			

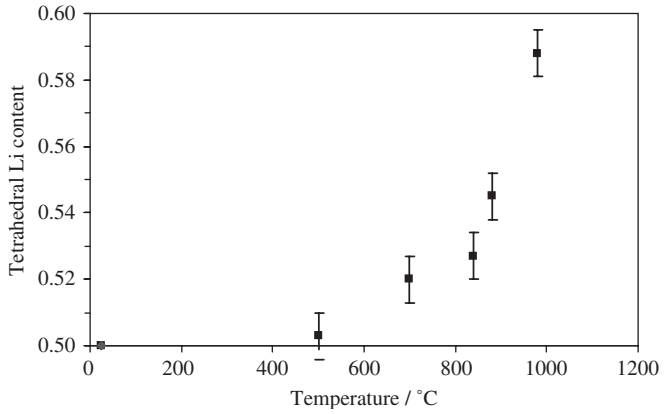

Fig. 6. Variation of refined Li fraction on the 8*c* site with temperature.

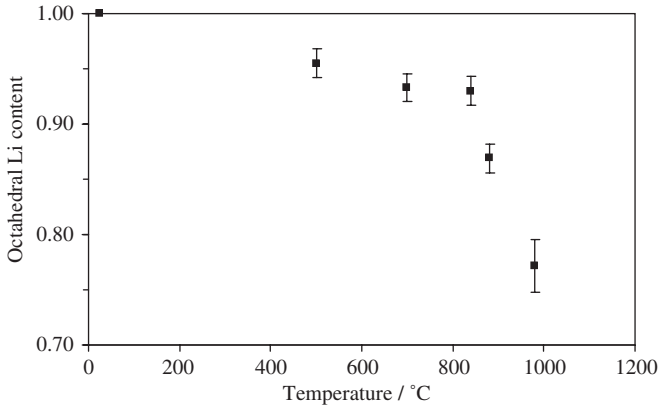

Fig. 7. Variation of refined Li fraction on the octahedral site(s) with temperature.

Spinels of type AB_2O_4 are generally described in terms of the arrangements of cations over the tetrahedral and octahedral interstices i.e., whether normal: $[A]^{tet}[B_2]^{oct}O_4$, inverse: $[B]^{tet}[A,B]^{oct}O_4$, or random: $[B_{0.67}A_{0.33}]^{tet}[A_{0.67}B_{1.33}]^{oct}O_4$. The degree of inversion may vary with composition and temperature for a given phase. A similar nomenclature can be used to describe the cation mixing in these ordered spinels, by using the general formula $[A_{2-i}B_i]^{tet}[A_iB_{1-i}]^{oct1}[B'_3]^{oct2}O_8$, where A = Li, B = Co, B' = Ti, i = degree of inversion (Table 3). The fully ordered ternary phase at room temperature can be regarded as inverse since $i = 1$; normal and random spinels have $i = 0$ and 0.67, respectively. The spinel composition moves towards being random as temperature increases, but the observed levels of cation mixing do not reach that of the fully random formula within the range of temperatures studied. Instead, the disordering transition becomes complete when the level of cation mixing reaches $i \approx 0.84$, i.e., the midway point between the fully ordered inverse phase and the fully random arrangement. Thus, Co still exhibits a strong preference for tetrahedral coordination, even at the highest temperatures studied.

The degree of scattering, S, from any given equivalent crystallographic site is the weighted average of the scattering factors of the atoms that occupy that site, i.e.,

$$S = xA + (1 - x)B,$$

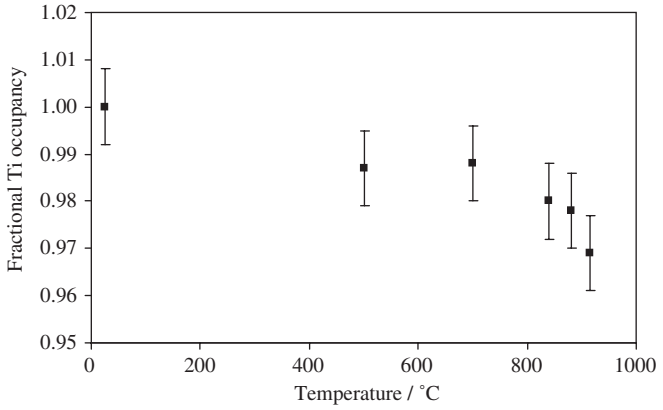

Fig. 8. Variation of refined Ti fraction on the 12*d* octahedral site with temperature.

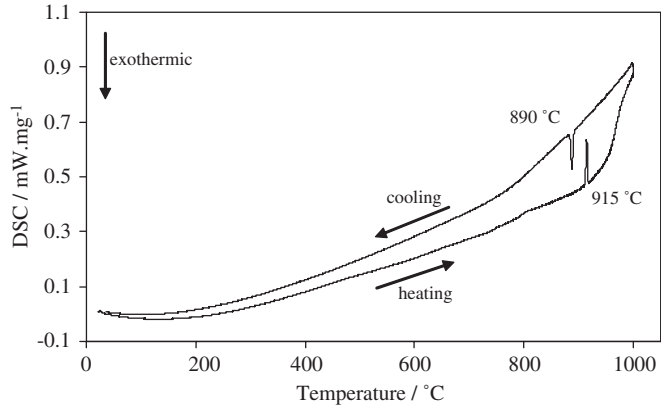

Fig. 9. Differential scanning calorimetry plot for $Li_2CoTi_3O_8$.

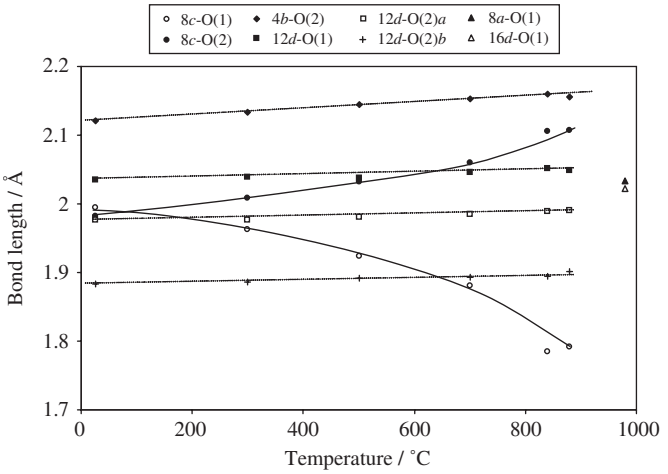

Fig. 10. Variation in calculated bond length with temperature for $Li_2CoTi_3O_8$. Dotted (for octahedral sites) and filled (for tetrahedral sites) lines included as a guide for the eye.

Table 3
Normal, random and inverse stoichiometry nomenclature for ternary spinel oxides; refined data from sample at 980 °C also shown

Cation distribution	Degree of inversion, *i*	Example stoichiometry
Normal	0	$[Li_2]^{tet}[Co]^{oct1}[Ti_3]^{oct2}O_8$
Random	0.67	$[Li_{4/3}Co_{2/3}]^{tet}[Co_{1/3}Li_{2/3}]^{oct1}[Ti_3]^{oct2}O_8$
Inverse	1	$[LiCo]^{tet}[Li]^{oct1}[Ti_3]^{oct2}O_8$
980 °C	0.84	$[Li_{1.16}Co_{0.84}]^{tet}[Li_{0.84}Co_{0.16}]^{oct1}[Ti_3]^{oct2}O_8$

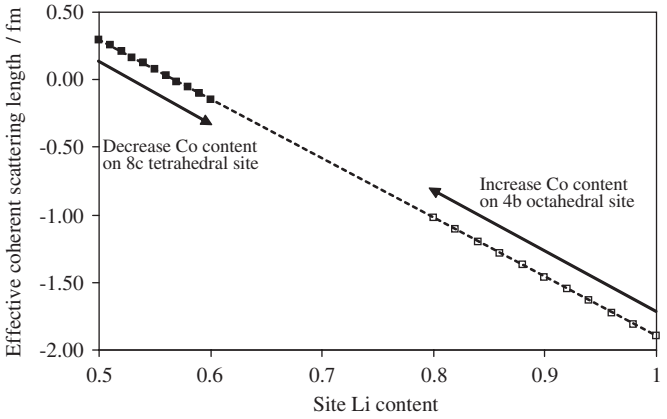

Fig. 11. Schematic diagram showing calculated effective bound average coherent scattering lengths for sites containing various ratios of Li and Co. Filled symbols represent Li content on the 8*c* tetrahedral site, while empty symbols represent Li content on the 4*b* octahedral site; for both interstices, the balance of the occupancy is filled to unity with Co.

where x $(1-x)$ represent the occupancies of atoms with scattering lengths A and B. Using this model, the levels of scattering calculated for various Li/Co arrangements are shown in Fig. 11. Since the coherent scattering lengths for Li (−1.90 fm) and Co (+2.49 fm) are of similar magnitude but different sign, the effect of having these cations on the same site is partial or complete cancellation. (For comparison, the scattering length for natural vanadium, generally considered 'invisible' to neutrons, is −0.38 fm.) Thus, for the tetrahedral site, the level of scattering is close to zero when the Li occupancy is between 0.55 and 0.59 which probably explains why full refinements could not be made for data collected over the range 890–930 °C. This also offers an explanation for the decrease in refined U_{iso}s; if the tetrahedral Li and Co are diverging onto two discrete but closely separated crystallographic sites, then the cancellation effect of their scattering lengths would be reduced; more scattering would be observed from this area of the structure. Refinement of U_{iso}s for an averaged Li/Co site would then decrease accordingly, as observed in our analyses, as the refinement program tries to model the additional scattering. The scattering on the octahedral site, Fig. 11, is always significant and it was always possible to refine the variable parameters for this site.

The refined fraction of Ti on the 12*d* site decreased by up to ~3% as a function of increasing temperature (Fig. 8). This is consistent with the introduction of a small amount

of Li and/or Co onto this site; the magnitudes of the coherent scattering lengths for Li and Co are smaller than that of Ti. So, we would expect to see a decrease in the level of scattering should either cation substitute onto this site. Refinements in which small amounts of Ti were placed on the 4*b* site were unsuccessful. Refinement of the occupancy of the 16*d* site at 980 °C were approached in two ways: (i) by including a fixed amount of Ti and refining the Li/Co content over the remainder of the site, and (ii) setting a fixed amount of Ti and refining its occupancy alone. The results from both approaches were consistent with the 16*d* site being filled with a disordered mixture of 0.75Ti and a 4:1 mix of Li and Co.

The nature of the order–disorder phase transition has been studied by two techniques. The DSC data are in agreement with previous work suggesting that the disordering process on heating contains a first-order component at ~915 °C. However, the Rietveld refinements show that disordering begins at ~500 °C, that the degree of cation mixing increases with further heating over an extended temperature range (~400 °C), and that cation mixing involves all cations in the structure. This suggests that the transformation commences as a second-order phase transition, which continues over a large temperature range and terminates with a first-order discontinuity.

7. Conclusions

A combination of Rietveld refinement of variable temperature ND and DSC data shows that $Li_2CoTi_3O_8$ exhibits an order–disorder transition on heating, involving a change in symmetry from the $P4_332$ space group to $Fd\bar{3}m$. This appears to be a second-order transition that culminates in a first-order discontinuity, since the disordering includes all of the cations disordering over all of the crystallographic sites continuously with increasing temperature.

Acknowledgments

We thank Dr. Ron Smith for his assistance with the neutron powder diffraction data collection, and Drs. Neil C. Hyatt, Gabrielle C. Miles, Emma E. McCabe and Karl R. Whittle for useful discussions and EPSRC for support.

References

[1] E.J.W. Verwey, E.L. Heilmann, J. Chem. Phys. 15 (4) (1947) 174–180.
[2] N.W. Grimes, Phys. Technol. 6 (1975) 22–27.
[3] A.N. Cormack, G.V. Lewis, S.C. Parker, C.R.A. Catlow, J. Phys. Chem. Solids 49 (1) (1988) 53–57.
[4] K.E. Sickafus, J.M. Wills, N.W. Grimes, J. Am. Ceram. Soc. 82 (12) (1999) 3279–3292.
[5] E. Kordes, Z. Krist. A 91 (1935) 193.
[6] P. Braun, Nature 170 (1952) 1123.
[7] H. Kawai, M. Tabuchi, M. Nagata, H. Tukamoto, A.R. West, J. Mater. Chem. 8 (5) (1998) 1273–1280.
[8] H. Kawai, M. Nagata, H. Kageyama, H. Tukamoto, A.R. West, Electrochim. Acta 45 (1–2) (1999) 315–327.
[9] P. Strobel, A.I. Palos, M. Anne, F. Le Cras, J. Mater. Chem. 10 (2) (2000) 429–436.
[10] A.R. West, H. Kawai, H. Kageyama, M. Tabuchi, M. Nagata, H. Tukamoto, J. Mater. Chem. 11 (6) (2001) 1662–1670.
[11] P. Strobel, A. Ibarra-Palos, M. Anne, C. Poinsignon, A. Crisci, Solid State Sci. 5 (7) (2003) 1009–1018.
[12] B. Antic, G.F. Goya, H.R. Rechenberg, V. Ksuigerski, N. Jovic, M. Mitric, J. Phys.: Condens. Matter 16 (2004) 651–659.
[13] H.M. Rietveld, J. Appl. Crystallogr. 2 (1969) 65.
[14] K. Hirota, M. Ohtani, N. Mochida, A. Ohtsuka, J. Ceram. Soc. Jpn. 96 (1998) 92.
[15] T. Saito, N. Mochida, A. Ohtsuka, Yogyo-Kyokai-Shi 95 (1987) 604.
[16] B.H. Toby, EXPGUI, a graphical user interface for GSAS, J. Appl. Crystallogr. 34 (2001) 210–213.
[17] A.C. Larson, R.B. Von Dreele, General structure analysis system (GSAS), Los Alamos National Laboratory Report LAUR 86–748, 2000.
[18] R.D. Shannon, C.T. Prewitt, Acta. Crystallogr. B 26 (1970) 1046.
[19] C. Masquelier, H. Kageyama, T. Takeuchi, Y. Saito, O. Nakamura, J. Power Sources 54 (1995) 448–451.
[20] V.S. Hernandez, L.M.T. Martinez, G.C. Mather, A.R. West, J. Mater. Chem. 6 (1996) 1533.